

Revisiting the interaction between Antarctic Sea ice and Southern Ocean cyclones

Article

Accepted Version

Zhong, R., Hodges, K. ORCID: <https://orcid.org/0000-0003-0894-229X>, Yang, Q. and Chen, D. (2025) Revisiting the interaction between Antarctic Sea ice and Southern Ocean cyclones. *Journal of Geophysical Research*, 130 (8). e2024JD042914. ISSN 2156-2202 doi: 10.1029/2024JD042914 Available at <https://centaur.reading.ac.uk/122379/>

It is advisable to refer to the publisher's version if you intend to cite from the work. See [Guidance on citing](#).

To link to this article DOI: <http://dx.doi.org/10.1029/2024JD042914>

Publisher: American Geophysical Union

All outputs in CentAUR are protected by Intellectual Property Rights law, including copyright law. Copyright and IPR is retained by the creators or other copyright holders. Terms and conditions for use of this material are defined in the [End User Agreement](#).

www.reading.ac.uk/centaur

CentAUR

Central Archive at the University of Reading

Reading's research outputs online

1 **Revisiting the Interaction Between Antarctic Sea Ice and Southern Ocean Cyclones**

2
3 **Rui Zhong¹, Kevin Hodges², Qinghua Yang^{1*}, and Dake Chen¹**

4
5 ¹ School of Atmospheric Science, Sun Yat-sen University, and Southern Marine Science and
6 Engineering Guangdong Laboratory (Zhuhai), Zhuhai, China.

7 ² National Centre for Atmospheric Science (NCAS) and Department of Meteorology, University of
8 Reading, Reading, United Kingdom.

9
10 Corresponding author: Qinghua Yang (yangqh25@mail.sysu.edu.cn)

11
12 **Key Points:**

- 13 • There is an inconsistent seasonal shift between storm track and sea ice edge.
- 14 • The high exposure areas of sea ice to cyclones are concentrated at the edges.
- 15 • Short-term sea ice responses various depends on the path and strength of cyclones.
- 16

17 **Abstract**

18 The sea ice around Antarctica undergoes a natural seasonal cycle of slow advance and
19 rapid retreat, which does not align with the seasonal north-south shift of the storm track over
20 the Southern Ocean. In particular, cyclones near the sea ice edge have a stronger impact on the
21 sea ice compared to those occurring elsewhere across the Southern Ocean. Despite the
22 increasing long-term trend of sea ice reversing after 2015, further investigation shows a
23 significant increase in the number of ice-linked cyclones in almost all subregions. To better
24 understand the seasonal and regional relationship between sea ice and cyclones, an exposure
25 index is introduced, encompassing various features of cyclones, local sea ice concentration (SIC),
26 and their interaction time. This index helps identify **key** seasons for each subregion. Analyzing
27 cyclones categorized by local SIC anomaly, we observe that cyclone strength and movement
28 direction significantly influence SIC anomalies. Composite results highlight the critical role of
29 temperature advection and surface sensible heat flux in SIC changes driven by cyclone circulation.
30 Though these results depend on the cyclone's interaction with the background circulation and its
31 position relative to the sea ice edge, they offer a new perspective on short-term sea ice changes
32 from a cyclone perspective **and improve the representation of cyclone-sea ice interactions in
33 climate models, enhancing predictions of future Antarctic sea ice trends.**

34

35 **Plain Language Summary**

36 As storm tracks in the Southern Ocean shift poleward due to climate change, more
37 cyclones are expected to impact Antarctic sea ice. This study specifically examines Southern
38 Ocean cyclones that affect sea ice, revealing that seasonal and regional differences in cyclone
39 characteristics shape the relationship between cyclones and sea ice. Composite results indicate
40 that variations in cyclone intensity and movement direction relative to the sea ice edge can
41 produce four distinct responses in local sea ice concentration, driven by the cyclonic wind field
42 and associated warm or cold air. This suggests that the short-term impacts of passing cyclones
43 on sea ice are not singular.

44

45 **1 Introduction**

46 Antarctic sea ice exhibits one of the largest seasonal signals on Earth, with significant
47 implications for the planetary albedo, energy exchange between the atmosphere and ocean,
48 thermohaline circulation, and ocean productivity (Eayrs et al., 2019, 2021; Clem et al., 2022). In
49 contrast to the consistent decrease in Arctic sea ice since 1978 (Serreze & Stroeve, 2015),
50 Antarctic sea ice has shown greater variability, with a dramatic trend reversal from growth to
51 decline since 2014 (Turner et al., 2017; Parkinson & DiGirolamo, 2016; 2021), and characterized
52 by strong regional and seasonal differences over the long term (Parkinson 2019; Eayrs et al.,
53 2021; Pirti et al., 2022). Current research has tried to understand these long-term and
54 asymmetric changes in Antarctic sea ice from both atmospheric and oceanic perspectives (Meehl
55 et al., 2019). However, there is still no consensus in explaining these observed changes (Hobbs et
56 al., 2016; Jones et al., 2016; Parkinson & DiGirolamo, 2021).

57 An increasing number of record low sea ice events have been observed in both
58 hemispheres since 2010, and extratropical cyclones have been considered to play an important
59 role in these events. In the Arctic, the 2012 record low Arctic sea ice cover was attributed to a
60 strong storm that entered the central Arctic in early August (Simmonds & Rudeva 2012).
61 Additionally, two August storms contributed to another record low in the Arctic in 2016 (Petty et
62 al., 2018). Strong storms can separate a small portion of the sea ice from the main ice pack and
63 cause further decay in the main pack by increasing its exposure to wind and waves (Parkinson &
64 Comiso 2013). The storm-induced enhanced oceanic mixing can also lead to bottom melt and a
65 significant decrease in ice volume (Zhang & Lindsay 2013). Similarly, in the Antarctic, strong
66 cyclones drove unprecedented ice loss in the Weddell Sea during the austral spring and summer
67 of 2016/17 by advecting multi-year ice northward into warmer and lower latitudes (Turner et al.,
68 2020). A few months later, strong cyclones further triggered the re-occurrence of the Maud Rise
69 Polynya in the 2017 austral winter (Francis et al., 2019). The large negative anomaly of sea ice
70 extent (SIE) in the Weddell Sea during April and May 2019 was caused by a series of intense and
71 explosive polar cyclones (Jena et al., 2022a). Record low sea ice events in other regions of
72 Antarctica have also been found to be linked to cyclone activity. For instance, a series of intense
73 polar cyclones in late 2021 resulted in a strong offshore flow and coastal polynya in the Ross Sea,
74 accelerating sea ice loss through increased solar radiation absorption and nonlinear ice-albedo
75 feedback, resulting in a record low in February 2022 (Turner et al., 2022; Wang et al., 2022). In
76 the extreme sea ice loss of 2023, cyclones intensified northerly winds and subsequently caused
77 a significant retreat in the Weddell Sea and Ross Sea (Jena et al., 2024). Although there is a
78 different land-sea distribution and more variable sea ice trends in the Southern Hemisphere
79 compared to that in the Northern Hemisphere, it appears that cyclones may play a crucial role in
80 modulating the SIE in the Southern Hemisphere as well.

81 High-latitude cyclones act as a bridge connecting hemisphere-wide climate variability and
82 sea ice in many complex ways (Yuan et al., 1999; Vihma 2014). Specifically, in low sea ice
83 concentration regions, the transfer of high amounts of latent and sensible heat to the
84 atmosphere would be expected to increase baroclinicity and promote the development of
85 atmospheric disturbances (Watkins & Simmonds, 1995). Thus, a decrease in SIE may increase the
86 number of cyclones (Simmonds & Wu 1993), which, in turn, could drive a southward shift of high-
87 latitude cyclones and potentially enhance downstream cyclone density (Pezza et al., 2008).
88 Although some studies suggest that atmospheric stresses and the topographic asymmetry of the
89 Antarctic continent (Howarth 1983; Godfred-Spenning & Simmonds 1996), instead of sea ice,
90 dominate the density and track of cyclones, less sea ice accompanied by changes in cold air
91 outbreaks and baroclinic properties do affect the storm track and cyclogenesis (Menéndez et al.,
92 1999; Yuan et al., 1999). On the other hand, strong winds related to cyclone systems may alter
93 the distribution of sea ice through advection and their impact of surface stress on the ice surface
94 (Watkins & Simmonds 1998), affecting the speed at which water in them refreezes (Dare &
95 Atkinson, 1999), roughing the older sea ice in the frontal ice zone (Nghiem et al., 2016) and
96 inducing a rapid growth of sea ice in specific regions (Wang et al., 2014). In addition to the effect
97 of wind, the cyclone-induced dynamic (poleward propagation of ocean waves and ice motion)
98 and thermodynamic (heat and moisture plumes from midlatitudes, ocean mixed layer warming)
99 processes can facilitate sea ice loss (Jena et al., 2022b). Hence, cyclones influence sea ice advance

100 and retreat differently across seasons (Finocchio et al., 2022). Even within a single season, Mundi
101 and L'Ecuyer (2024) observed that the increased frequency of early summer storms, which drive
102 greater ice loss, has resulted in a more pronounced decline in the MIZ ice area compared to the
103 1980s. Furthermore, their findings indicate that southerly wind-enhancing summer storms in the
104 Arctic typically reduce ice area, whereas northerly storms tend to increase it. In addition to their
105 significant impact on the marginal ice zone (Finocchio et al., 2020; Vichi et al., 2019), cyclones
106 contribute to polynya formation through atmospheric and oceanic processes (Francis et al., 2020;
107 Jena et al., 2024) and influence sea ice production within polynyas (Wang et al., 2021; 2023).

108 Variability in Antarctic sea ice and cyclones have been linked in previous studies (Carleton
109 1983; Howarth 1983; Streten 1983). The correlation between sea ice and cyclones varies in
110 different regions and over time (Carleton 1983; Howarth 1983). On an interannual timescale,
111 positive sea ice anomalies and cold air outbreaks are closely associated with the occurrence of
112 cyclones (Carleton & Carpenter 1989). The development and maintenance of sea ice anomalies
113 have also been found to be significantly affected by the track, intensity, and frequency of cyclones
114 (Streten 1983). However, due to the limited availability of observational records, conclusions of
115 these earlier studies may only apply to specific periods and lack general applicability. Benefiting
116 from the development and application of cyclone tracking algorithms, Simmonds and Wu (1993)
117 found that less Antarctic sea ice leads to lower sea-level pressure as a result of more cyclones
118 but not necessarily more intense ones. The relationship between Antarctic sea ice and Southern
119 Ocean cyclones is regionally dependent, and not consistent across the entire sea-ice zone on a
120 seasonal time scale (Godfred-Spenning & Simmonds 1996). Their correlation is more significant
121 near the sea ice edge (Simmonds 2003). Local cyclone density appears more closely linked to sea
122 ice upstream or downstream, indicating the crucial role of the 10-m wind associated with the
123 synoptic system in the sea ice variability (Schemm 2018). In addition, the relationship also
124 depends on the spatial and temporal scale. There are weak correlations on interannual
125 timescales but the correlations become strong when sea ice lags both track density and
126 cyclogenesis by one season (Godfred-Spenning & Simmonds 1996; Simmonds 1996). Zhang et al.
127 (2023) found that this lag time is 1-2 months in austral summer using the lagged maximum
128 covariance analysis (MCA). The above studies focus on the correlation between cyclone density
129 and sea ice extent on different timescales and regions, but most of them barely achieve statistical
130 significance. They also lack a reasonable explanation for the significant correlation and it is still a
131 puzzle about the significant correlations only occur in particular seasons and regions. Cyclones
132 with different paths and genesis locations exhibit varying meridional moisture and momentum
133 fluxes (Sinclair & Dacre 2019; Ward et al., 2023), causing vary impacts on sea ice. Such details are
134 hidden within the cyclone track density and result in producing a weak correlation between sea
135 ice and cyclones. Recent findings reveal that 30-40% of extreme sea ice variability events on
136 synoptic timescales are linked to Southern Ocean cyclones, with the characteristics of these
137 cyclones playing a significant role in shaping their relationships in different regions (Hepworth et
138 al., 2024).

139 Although there is a tug of war in the shift of the westerly jet stream in the Southern
140 Hemisphere due to the ozone-hole recovery and increasing greenhouse gases (Perlwitz 2011), a
141 confirmed poleward shift of the storm track can be seen in the Southern Hemisphere both in the
142 historical record (Bender et al., 2012) and in future simulations (Tamarin-Brodsky & Kaspi 2017;

143 Priestley & Catto 2021). More cyclones moving closer to the Antarctic continent are likely to
144 intensify their impact on sea ice distribution and variability. In this context, focusing on ice-linked
145 cyclones (near or over the sea ice) will be crucial for understanding their role in shaping future
146 sea ice dynamics. At present, we have access to comprehensive and reliable data for the Antarctic
147 sea ice edge and sea ice concentration since 1979 from passive microwave satellites and high-
148 resolution reanalysis data, as well as datasets of Southern Ocean cyclone tracks produced by
149 applying objective tracking algorithms to reanalysis data. The aim of this paper is to provide a
150 clearer picture of the interaction of cyclones with sea ice through addressing the following
151 questions:

152 (1) What are the characteristics and trends of ice-linked cyclones?

153 (2) What are the mechanisms for the different responses of SIC to cyclones?

154 The paper continues as follows: Section 2 describes the reanalysis data, sea ice data,
155 cyclone tracking method, and a sea ice exposure index used in this study. The climatology of ice-
156 linked cyclones and the composite results for different types of cyclones are presented in Section
157 3. Discussion and conclusions are provided in Sections 4 and 5.

158

159 **2 Data and Methods**

160 2.1 Sea ice and reanalysis data

161 We use atmospheric and oceanic data from the European Centre for Medium-Range
162 Weather Forecasts (ECMWF) fifth-generation reanalysis data (ERA5, Hersbach et al., 2020),
163 including sea ice concentration (SIC), mean sea level pressure (MSLP), and relative vorticity at
164 850 hPa (VORT850). The ERA5 reanalysis data have an original spectral resolution of triangular
165 truncation 639 (T639, ~31 km horizontal resolution) and 137 hybrid sigma vertical levels. The
166 data are available at a 0.25-degree horizontal resolution and hourly temporal resolution since
167 1940. In this study, we specifically analyze the data starting from 1980 to align with the sea ice
168 data from satellite observations. The European Organization for the Exploitation of
169 Meteorological Satellites (EUMETSAT) Ocean and Sea Ice Satellite Application Facility (OSI SAF)
170 reanalysis product (v409a; Eastwood et al., 2014), various versions of the HadISST2 sea ice
171 product (Titchner & Rayner, 2014) and the operational OSI SAF product that is also part of the
172 OSTIA product were considered for the SIC data of ERA5 (Hirahara et al., 2016; Hersbach et al.,
173 2020), which have been widely used in previous studies (Aue et al., 2022; Jenkins et al., 2022;
174 Hepworth et al., 2024). It should be noted that the hourly SIC data from ERA5 are updated daily
175 but stored at hourly frequency to align with the atmospheric data.

176 The sea ice edge is often defined as the outermost boundary separating the open ocean and
177 sea ice, represented by the 15% SIC contour (Goessling et al., 2016; Zampieri et al., 2019).
178 However, its precise location can be influenced by factors such as islands in the Southern Ocean,
179 polynyas, and semi-enclosed open water. Therefore, to address these challenges, we define a
180 conservative sea ice edge by extending it southward by more than 0.5° latitude from the 15% SIC
181 contour line. To better capture the north-south variability of the sea ice edge, we introduce the
182 latitude of the ice edge (IEL) as a metric to represent its position. Subsequently, we calculate the

183 average latitude of hourly sea ice edge to obtain daily, monthly, seasonal, and yearly sea ice edge
184 positions. Additionally, the corresponding variance is computed to quantify its interannual
185 variability. Considering the trend reversal observed around 2015, we further calculate the
186 regional IEL trends for two distinct periods, 1980-2015 and 1980-2022, following the
187 methodology proposed by Maksym (2019).

188

189 2.2 Cyclone tracking

190 Using the 850 hPa relative vorticity data from ERA5 reanalysis, we track the Southern
191 Ocean cyclones from 1980 to 2022 using the objective tracking algorithm TRACK (Hodges 1994,
192 1995, 1999). To better leverage ERA5's high temporal resolution for cyclone tracking, we selected
193 a temporal resolution of 1 hour and the spatial resolution of T42 (~310 km at the equator) after
194 evaluating alternative spatial-temporal schemes (Zhong et al., 2022). The tracking process
195 consists of three steps: spectral filtering to reduce noise in the vorticity field and to focus on
196 synoptic scale cyclones, cyclone center positioning by finding the off-grid vorticity minima, and
197 optimal track construction by minimizing a cost function for track smoothness constructed from
198 changes in direction and speed subject to adaptive constraints. Tracks are filtered post-tracking
199 to retain cyclone tracks with a minimum lifespan of 2 days and a movement distance of over 1000
200 km. These criteria effectively exclude short-lived or unrealistic systems (Uotila et al., 2011). Full
201 details of the tracking are given in Zhong et al. (2022). The higher temporal resolution enables
202 accurate identification of the cyclones' initial and final track points, particularly useful for locating
203 the cyclone center over the sea ice, determining the speed and moving direction of cyclones, and
204 measuring the interaction time between the cyclone and sea ice. The spectral filtering of T42 will
205 **exclude** small-scale and mesoscale cyclones that have a different climatological distribution from
206 the synoptic-scale cyclones (Stoll 2022).

207 In addition, the full-resolution MSLP minima is added to the vorticity tracks and used as
208 the reference of the intensity of the cyclones. TRACK achieves this by searching for the nearest
209 minima within a 5° radius (geodesic) of the vorticity center. If a true MSLP minimum cannot be
210 found (such as open cyclones that has no closed isobaric line), the MSLP value at the location of
211 vorticity center is taken. A similar method can be used to search for the maximum SIC for each
212 track point within a 5° radius, which facilitates the distinction between ice-linked and non-ice-
213 linked track points

214 The axis of the storm track refers to the maximum track density of Southern Ocean
215 cyclones. The latitude of this axis will be used to calculate the relative distance with sea ice edge.
216 Specifically, we also defined the number of track points within a 500 km radius (Haversine
217 distance) at each grid point as the feature density, highlighting the areas of most frequent cyclone
218 activity. It is note that feature density is different from track density because track points are
219 counted on multiple grid points in feature density but once in track density.

220 The Southern Ocean is divided into five subregions (Ionita et al., 2018; Turner et al., 2017):
221 Indian Ocean (IO: 20°E-90°E), Western Pacific Ocean (WPO: 90°E-160°E), Ross Sea (RS: 160°E-
222 130°W), Amundsen-Bellingshausen Sea (ABS: 130°W-60°W), and Weddell Sea (WS: 60°W-20°E).
223 We further categorize the track points into two groups based on their relative distance from the

224 sea ice edge. The "inside" group comprises track points located within (south of) the sea ice edge,
 225 over the sea ice but not on land. The "outside" group contains track points located outside (north
 226 of) the sea ice edge, but with a relative distance of less than 5° of latitude to the ice edge. They
 227 will be called inside cyclones and outside cyclones respectively in the rest of the paper. This
 228 approach excludes cyclones that are distant from the sea ice and allows an analysis of the
 229 differences in the behavior of cyclones inside and outside the ice edge, as well as their respective
 230 impacts on the sea ice. It provides a possible to investigate the differences in the number and
 231 characteristics of cyclones arriving at the sea ice edge and entering the interior of the sea ice
 232 edge, offering a more detailed understanding of cyclones in the ice zone. The choice of 5° is based
 233 on findings by Simmonds (1996), who observed significant correlations between sea ice and
 234 cyclone density within relatively short distances. Here, 5° is a typical mean radius of extratropical
 235 cyclones although some cyclones may have longer fronts.

236 Cyclone-centered composites are performed on the re-gridded field to avoid the effects
 237 of meridional convergence in polar regions. The compositing domain extends 20° in all four
 238 cardinal directions, centered on the cyclone's vorticity center at 850hPa level. This rectangular
 239 domain is initially defined at the equator and then rotated to the cyclone center using a rotation
 240 matrix to maintain a fixed aspect ratio in meridional and zonal directions. Then, the factors fields
 241 are interpolated onto the grid using B-spline interpolation. Using a domain based on geographic
 242 coordinates makes it easier to identify direction and relative distance than a circular polar
 243 coordinate composite or a distance–azimuth radial domain used in other studies (Rudeva and
 244 Gulev 2011; Catto 2018; Ponce de León and Bettencourt 2021; Clancy et al., 2022). In particular,
 245 there is a land mask for the temperature advection at 10m level, reducing noise in the composite
 246 field. To minimize interference from upstream and downstream cyclones in the composite results,
 247 this study selects only isolated cyclones for analysis. An isolated cyclone is defined as one with
 248 no other cyclones present within 20° to the east or west.

249

250 2.3 Exposure index

251 The impact of cyclones on sea ice is significant and depends on its concentration. Regions
 252 with lower SIC, such as the marginal ice zone, are more significantly affected than those with
 253 higher concentrations. The number, intensity, and relative distance of passing cyclones all
 254 influence the underlying sea ice to different degrees. To comprehensively assess the impact of
 255 cyclone activity on sea ice, we have developed an exposure index for each grid point (x, y) at
 256 time t is calculated as:

$$257 \quad Exposure(x, y, t) = \frac{1}{SIC(x, y, t)} \sum_{t-24}^{t+24} \sum_{n=1}^{n=m} \frac{Nor_Strength(t)}{Nor_Distance(t)+\varepsilon},$$

258 where $\varepsilon = 10^{-4}$ is used to avoid division by zero. m represents the total number of track
 259 points within a 5° radius of the sea ice grid point over a 2-day period.

$$260 \quad Nor_Strength(t) = \frac{Strength_{case(t)} - Strength_{min}}{Strength_{max} - Strength_{min}},$$

261 where $Nor_Strength(t)$ is the normalized intensity (MSLP) of the cyclones, with a min-
 262 max normalized to a range of 0~1.

263

264 Since higher intensity corresponds to a greater value, we take a negative value for the
 265 mslp value at the center of the cyclone. $Strength_{case(t)}$ is the strength of cyclones at each
 266 timestep. $Strength_{max}$ and $Strength_{min}$ are the maximum and minimum strength of cyclones
 267 in the dataset, respectively.

268 The relative distance between the sea ice grid point and the cyclone center is denoted by
 269 a $Distance(t)$, normalized by a maximum distance of 500 km to remove its dimensionality and
 270 ensure its value is between 0 and 1.

$$271 \quad Nor_Distance(t) = \frac{Distance(t)}{500 \text{ km}},$$

272 To avoid division by zero when the distance between a cyclone and the sea ice grid point
 273 is zero, a small constant $\epsilon = 10^{-4}$ is added to the denominator. This adjustment ensures the
 274 correctness of calculations without significantly affecting the results.

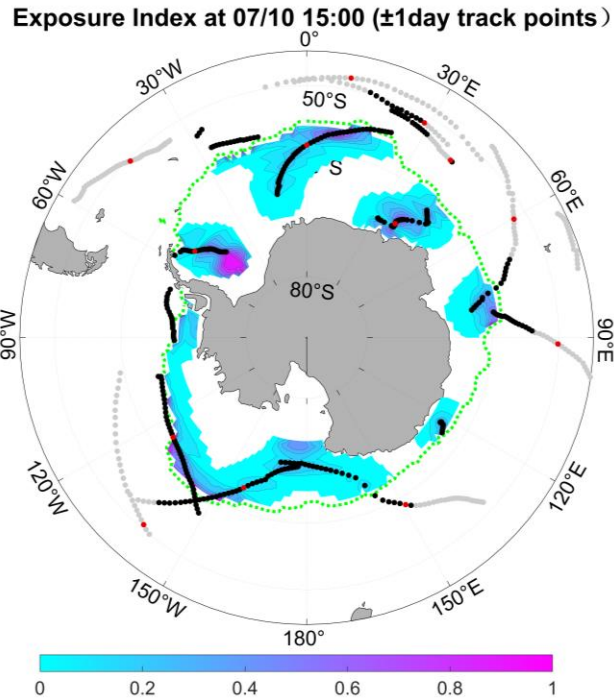
275 The SIC value of the sea ice at grid point (x, y) and time t is denoted as $SIC(x, y, t)$. Only
 276 the grid points with $SIC \geq 15\%$ will be used to calculate exposure index. To calculate the exposure
 277 of the local sea ice grid point to passing cyclones within a specific time period, we sum the
 278 contributions of all n cyclones that pass through a 500 km radius of the grid point from 120 hours
 279 before to 120 hours after each timestep (per hour). This summation results in the index that
 280 quantifies the exposure of each sea ice grid point to passing cyclones at any moment. The
 281 exposure index is influenced by factors such as cyclone intensity ($Strength_{case(t)}$), distance from
 282 the cyclone to the sea ice grid point ($Distance(t)$), the number of cyclones within a 500 km
 283 radius ($\sum_{n=1}^{n=m}$) in a period (\sum_{t-24}^{t+24}), and the local SIC ($SIC(x, y, t)$). The interaction time
 284 between sea ice and cyclones is represented by the sum of times ($\sum_{t-24}^{t+24} \sum_{n=1}^{n=m}$) and the strength
 285 of cyclones over the sea ice is also computed in a 2-day period ($\sum_{t-24}^{t+24} \sum_{n=1}^{n=m} Strength_{case(t)}$).

286 In order to better compare the results between seasons, the exposure index at each time
 287 point is also normalized, with a min-max normalized to a range of 0~1.

$$288 \quad Nor_Exposure(t) = \frac{Exposure(x,y,t) - Exposure_{min}}{Exposure_{max} - Exposure_{min}},$$

289 The maximum and minimum exposure values are derived from all grid points with SIC
 290 $\geq 15\%$ over the entire 43-year period. The selected time window of ± 1 day (48 hours) aims to
 291 capture as many passing cyclones as possible. This window is subjectively chosen and can be
 292 extended to ± 3 or ± 5 days, as shown in sensitivity tests (Figures S1 and S2). Cyclone speed
 293 indirectly affects the exposure index by influencing both the number of cyclones and their
 294 interaction time with sea ice. Thus, the exposure index serves as a valuable metric for quantifying
 295 cyclone influence on local sea ice and exploring regional differences in this relationship. Figure 1
 296 illustrates $Nor_Exposure(t)$ at 15:00 on October 7, 2022, along with cyclone tracks over this 2-
 297 day period as an example.

298
 299

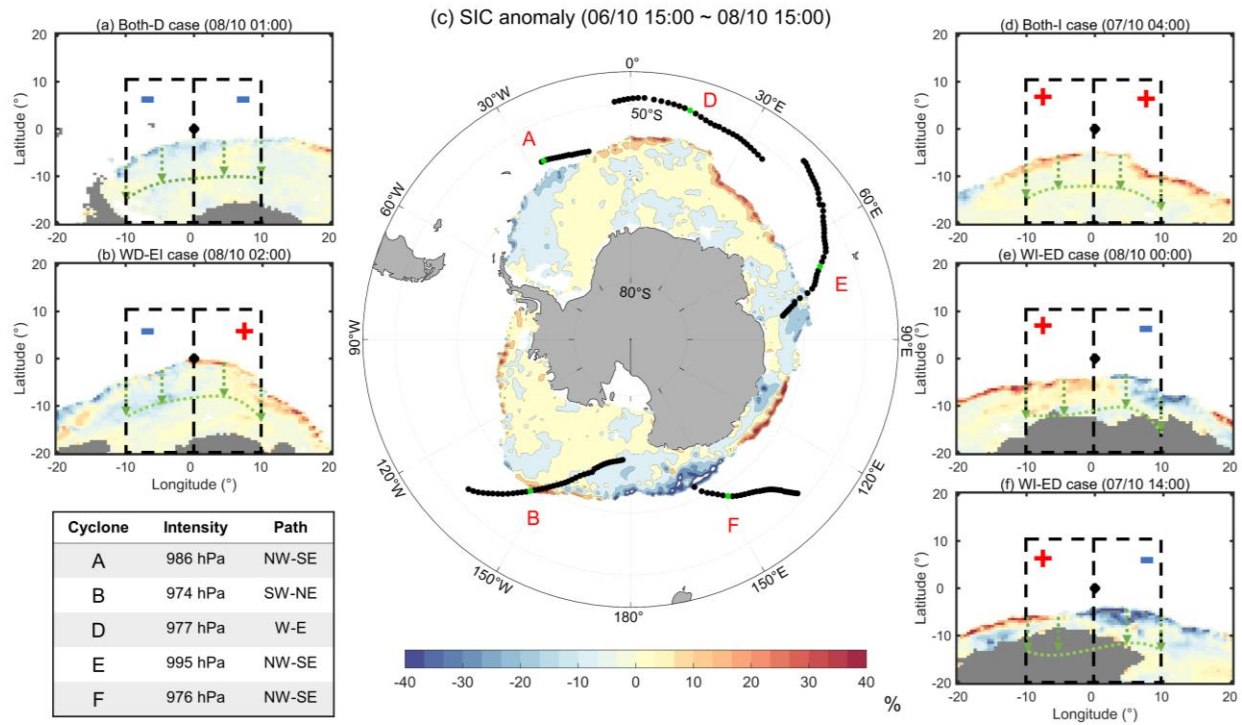


300

301 **Figure 1.** Normalized Exposure Index at 15:00 on October 7, 2022. Cyclone tracks are represented
 302 by dots. Gray dots represent cyclone track points far from the sea ice edge (green dashed line),
 303 while black dots indicate track points with sea ice within a 5° radius. Red dots mark the locations
 304 of cyclones at 15:00 on October 7, 2022.

305 2.4 Different sea ice response

306 The SIC anomaly field is re-gridded around the cyclone centers using B-spline
 307 interpolation to minimize the effects of meridional convergence in high latitudes. The SIC
 308 anomaly at each timestep is calculated as the difference between SIC values one day before and
 309 one day after. The mean SIC anomaly within 5° inward from the sea ice edge (indicated by the
 310 green dashed line) is calculated for a box region located to the west and east of the cyclone
 311 centers, as shown in Figure 2. This approach focuses on the main changes in the edge area and
 312 accommodates varying sea ice shapes. Based on the dominant anomalies observed on both sides
 313 of the cyclone, the cyclones are categorized into four groups: Both-I (SIC increase on both sides),
 314 Both-D (SIC decrease on both sides), WI-ED (SIC increase in the west and decrease in the east),
 315 and WD-EI (SIC decrease in the west and increase in the east). The SIC anomaly quantities for
 316 each cyclone are shown in Figure S3. The SIC changes on either side of the cyclone can reach up
 317 to 40%, with seasonal variations in the average SIC changes.



318

319 **Figure 2.** A schematic representation of four types of SIC responses to cyclones. (a) Both-D case
 320 (SIC decrease on both sides); (b) WD-EI case (SIC decrease in the west and increase in the east);
 321 (c) all cyclones with at least a 5% SIC anomaly from October 6 to October 8, 2022, with shaded
 322 areas indicating the SIC anomaly during the same period; (d) Both-I case (SIC increase on both
 323 sides); (e) and (f) WI-ED cases (SIC increase in the west and decrease in the east). The region
 324 between the sea ice edge and the green dashed line is used to calculate the mean SIC anomaly
 325 on the west or east flanks of cyclones. The intensity and path information for the five cyclone
 326 cases are summarized in the table.

327

328 3 Results

329 3.1 Variations in Antarctic sea ice and Southern Ocean cyclones

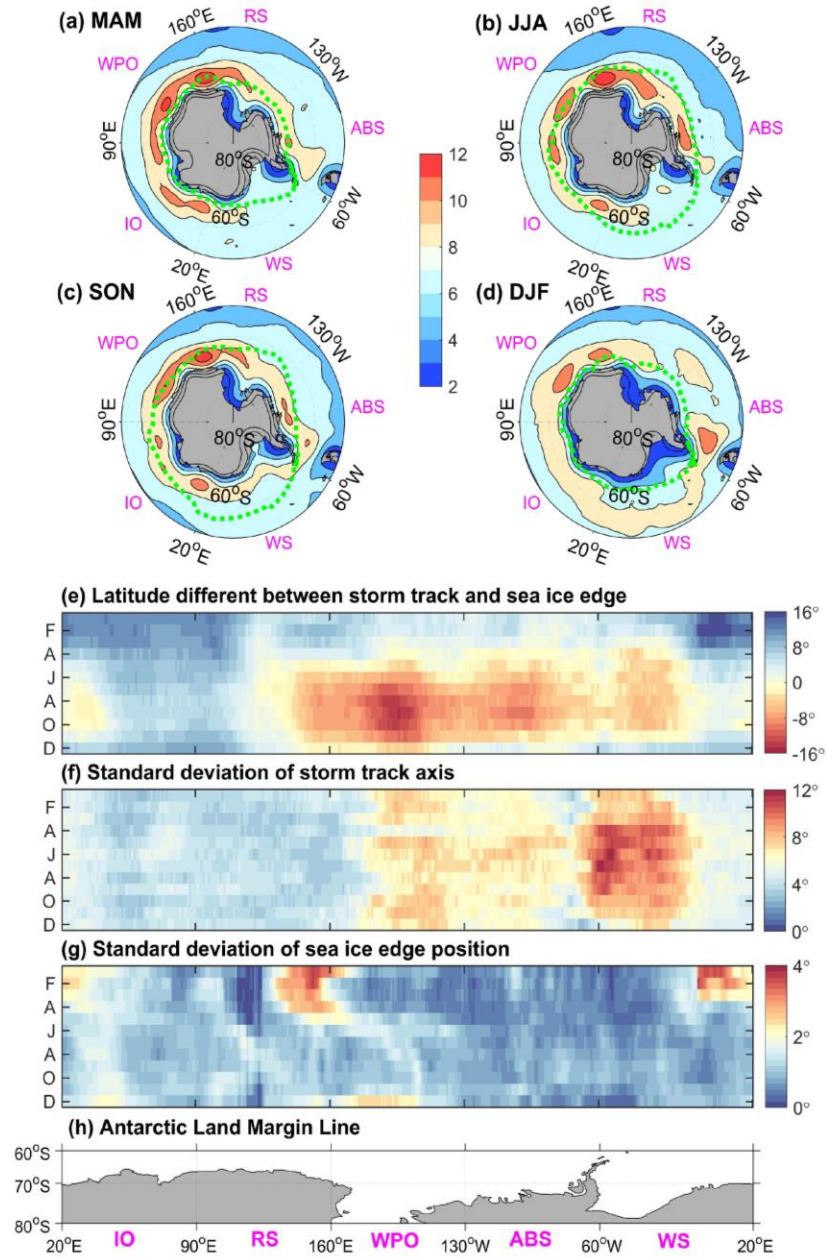
330 Antarctic sea ice undergoes a natural cycle characterized by gradual expansion and rapid
 331 retreat. The northward extension of the sea ice edge occurs from March to September, followed
 332 by a poleward retreat from October to February of the following year (Eayrs et al., 2019). This
 333 pattern results in a larger expanse of sea ice during winter (JJA) and spring (SON), and a smaller
 334 coverage during summer (DJF) and autumn (MAM), as shown in Figure 3a-d. Notably, regional
 335 differences exist in the seasonal shifts of sea ice extent. For example, the sea ice edge in the
 336 Weddell Sea (60°W-0°), Lazarev Sea (0-14°E), and Ross Sea (158°E-170°W) experiences more
 337 significant north-south seasonal variation compared to the IO and WPO sectors. These regions
 338 also exhibit larger standard deviations in the monthly positions of the sea ice edge (Figure 3g).
 339 The movement of sea ice in these areas is significantly influenced by katabatic winds and barrier

340 winds, which promote both sea ice production and export. However, their northward expansion
341 is constrained by the oceanic frontal zone and storms (Nghiem et al., 2016).

342 The feature density of Southern Ocean cyclones exhibits a circular pattern (Figure 3a-d),
343 gradually increasing from lower to higher latitudes. The highest cyclone frequency is observed
344 around 60°S, gradually decreasing closer to the Antarctic continent. Peak storm activity occurs in
345 the Indian Ocean and Western Pacific sectors year-round, consistent with the findings of Hoskins
346 and Hodges (2005). Additionally, both the location and intensity of the storm track exhibit
347 seasonal variation. During the retreat of sea ice (Figure 3c-d), the storm track shifts closer to the
348 Antarctic continent, with heightened cyclone activity along the coast. As the sea ice advances
349 (Figure 3a), the storm track shifts northward, particularly in the ABS and WS sectors, where it
350 extends as far north as 60°S and 55°S, respectively. However, in the IO and WPO sectors, the
351 location of the storm track remains relatively stable year-round, centered around 60°S.

352 Therefore, it is not surprising that the north-south movement of storm tracks over the
353 Southern Ocean does not align with the expansion and retreat of the sea ice edge (Figure 3e).
354 The storm track axis intersects the sea ice edge twice in the RS, ABS, and western WS in May and
355 November, resulting in disparities in the number of cyclones (track points) located inside and
356 outside the sea ice edge. The largest positive difference is observed in the 0-110°E region during
357 MAM and remains positive year-round, while the central RS and ABS regions exhibit the largest
358 negative difference in ASO, along with a significant inconsistent shift in the storm track and sea
359 ice edge, with a relative distance ranging from -10° to 17° latitude. Note that this difference is
360 heavily influenced by the position of the storm track, as the positions of the storm track in the
361 WPO, ABS, and WS regions exhibit significant variability (Figure 3f), which is greater than that at
362 the sea ice edge.

363 Given that cyclones with varying relative distances may have different impacts on sea ice,
364 their relationship is also influenced by the differing proportions of cyclones inside and outside
365 the sea ice edge. Therefore, it is valuable to categorize cyclone tracks located close to the sea ice
366 edge, rather than considering cyclones spanning the entire Southern Ocean. The precise selection
367 and classification of sea ice-linked cyclones based on their relative distance from the sea ice
368 provide a new perspective on the trends and variations of cyclones associated with sea ice, in the
369 context of global warming and the poleward movement of storm tracks.



370

371 **Figure 3.** (a–d) Seasonal feature density of Southern Ocean cyclones (shaded) and the mean sea
 372 ice edge (SIC ≥ 0.15 , green contour). Unit: per season. (e) Monthly variation in the latitudinal
 373 difference between the storm track axis (latitude of maximum density in each meridian) and the
 374 sea ice edge at the same longitude, calculated as the former minus the latter. (f) Monthly
 375 variation in the standard deviation of the storm track axis. (g) Monthly variation in the standard
 376 deviation of the sea ice edge position. (h) The edge of the Antarctic continent.

377

378 3.2 Trends of sea ice and ice-linked cyclones

379 The expansion of Antarctic sea ice might increase its interaction with mid-latitude
380 cyclones. Our analysis reveals that the average latitude of the full tracks of ice-linked cyclones,
381 as well as their tracks over ice, follows the trends of sea ice edge movement—showing a
382 northward shift before 2014 and a southward shift afterward. However, the trends in the average
383 latitude of cyclone genesis and lysis differ from those of sea ice (not shown).

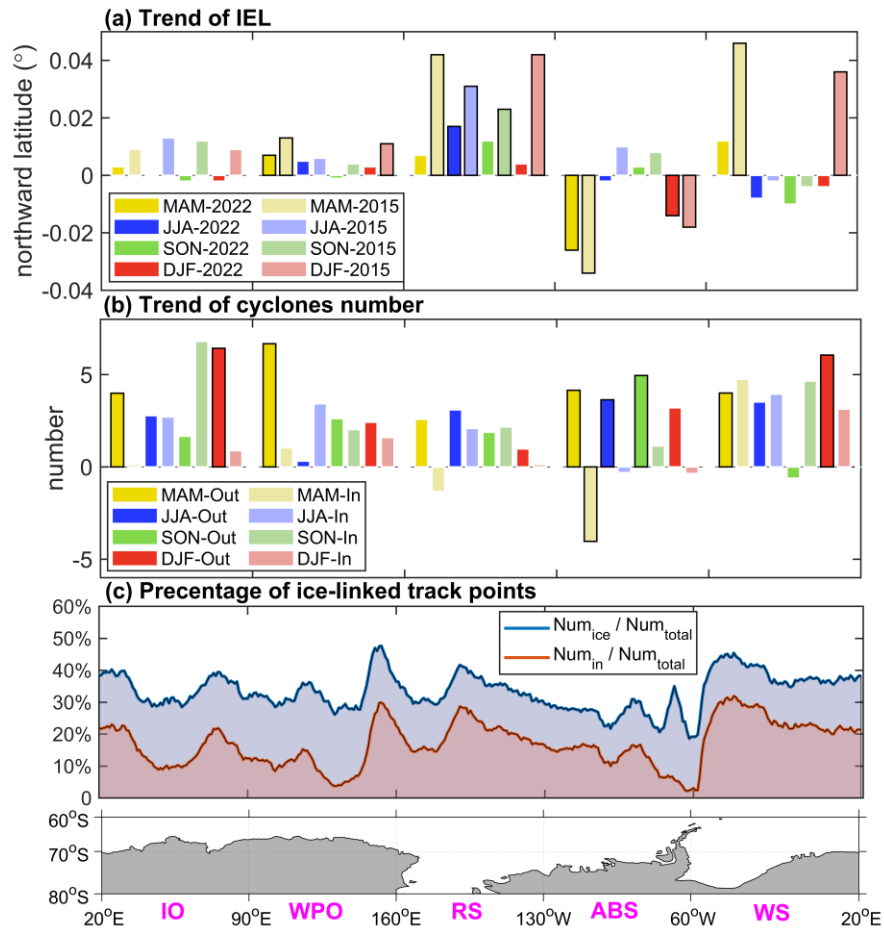
384 Further examining the latitude of the sea ice edge (IEL) within each sub-region, we find
385 more pronounced trends before 2015 than over the entire period from 1980 to 2022 (Figure 4a).
386 Some significant trends from 1980 to 2015, such as the northward shift of IEL in the RS region,
387 lose their statistical significance when data is extended to 2022. However, the southward IEL
388 trend in ABS during DJF and MAM, as well as the northward trend in WPO (RS) during MAM (JJA),
389 remain significant after 2015, consistent with previous studies (Maksym 2018). Notably, the
390 largest northward trends in RS have weakened, while those in WS have reversed southward. IEL
391 trends in IO and WPS are relatively small, indicating that inter-decadal variations in Antarctic sea
392 ice extent are primarily driven by the southward trend in ABS and the northward trend in RS.

393 Regional sea ice trends are driven by atmospheric and oceanic processes. The summer
394 Ross Sea decline is linked to an enhanced anticyclonic SAM pattern, while strengthened SAM
395 asymmetry in winter and spring influences SIC changes across Antarctica (Schroeter et al., 2023).
396 The extreme El Niño (Dec 2015–Feb 2016) triggered persistent ocean warming in the
397 Bellingshausen, Amundsen, and eastern Ross Seas (Stuecker et al., 2017; Parkinson, 2019). Sea
398 surface temperature (SST) trends are also consistent with the reversal of sea ice trends in these
399 regions. However, in Weddell Sea and some areas of the East Antarctica, sea ice changes are
400 mainly driven by weather-scale and teleconnection processes, with limited influence from large-
401 scale SAM variations (Schroeter et al., 2023).

402 Therefore, investigating the trend of ice-linked cyclones around Antarctica is crucial. In
403 Figure 4c, about 40% of the tracks of Southern Ocean cyclones will affect the sea ice and half of
404 them will enter the sea ice edge. The percentage is different across subregions but positive trends
405 are observed in the number of ice-linked cyclones in most regions (Figure 4b), particularly during
406 the MAM and DJF when the sea ice extent is relatively small (Figure 3a and 3d). The WS sector
407 exhibits the largest increase in cyclone numbers, while the RS has the smallest and non-significant
408 trend for all four seasons. Notably, the outside cyclones in the ABS region also have a significant
409 increasing trend in JJA and SON, which is not seen anywhere else in these seasons. Only the ABS
410 region exhibits a significant decreasing trend in the number of inside cyclones in MAM, which
411 might be associated with the southward trend of IEL in ABS. Predictably, the retreat of the sea
412 ice edge leads to a reduction in the number of cyclones within ice-covered areas. However, this
413 common assumption may not be true for the RS and WS regions. For example, the IEL in the WS
414 region shows a weak southward trend, yet there is still a positive trend in the number of inside
415 cyclones in this region, indicating cyclones may be moving southward in concert with the
416 southward-moving ice edge.

417 On a decadal timescale, increasing trends are observed in both the number of outside
418 and inside cyclones, while sea ice extent shows an increasing trend in the IO, WPO, and RS
419 regions, but a decreasing trend in the ABS and WS regions. Significant correlations are found

420 only between the IEL and the number of inside cyclones (not shown), rather than with outside
 421 cyclones. This suggests that no meaningful statistical relationship exists on a decadal timescale,
 422 even though the cyclones were well-tracked and selected. Instead, the relationship between
 423 cyclones and sea ice may be significant only on shorter timescales in specific regions. The
 424 regional and seasonal variations in ice-linked cyclone characteristics and sea ice conditions
 425 further complicate their relationship. Understanding both cyclone characteristics and regional
 426 sea ice variability is essential for addressing this issue.



427

428 **Figure 4.** (a) Trends in the latitude of the sea ice edge in each subregion from 1980 to 2015 (light-
 429 colored bars) and 2022 (dark-colored bars). Positive (negative) values indicate a northward
 430 (southward) shift trend. (b) Trends in cyclone frequency inside and outside the sea ice edge
 431 in each subregion from 1980 to 2022. Bars indicating significant trends are outlined in black (t-
 432 test: 95% confidence level). (c) The blue line represents the percentage of ice-linked track points
 433 at each meridian relative to all track points. The red line represents the percentage of track points
 434 inside the sea ice edge.

435

436 3.3 Features of ice-linked cyclones

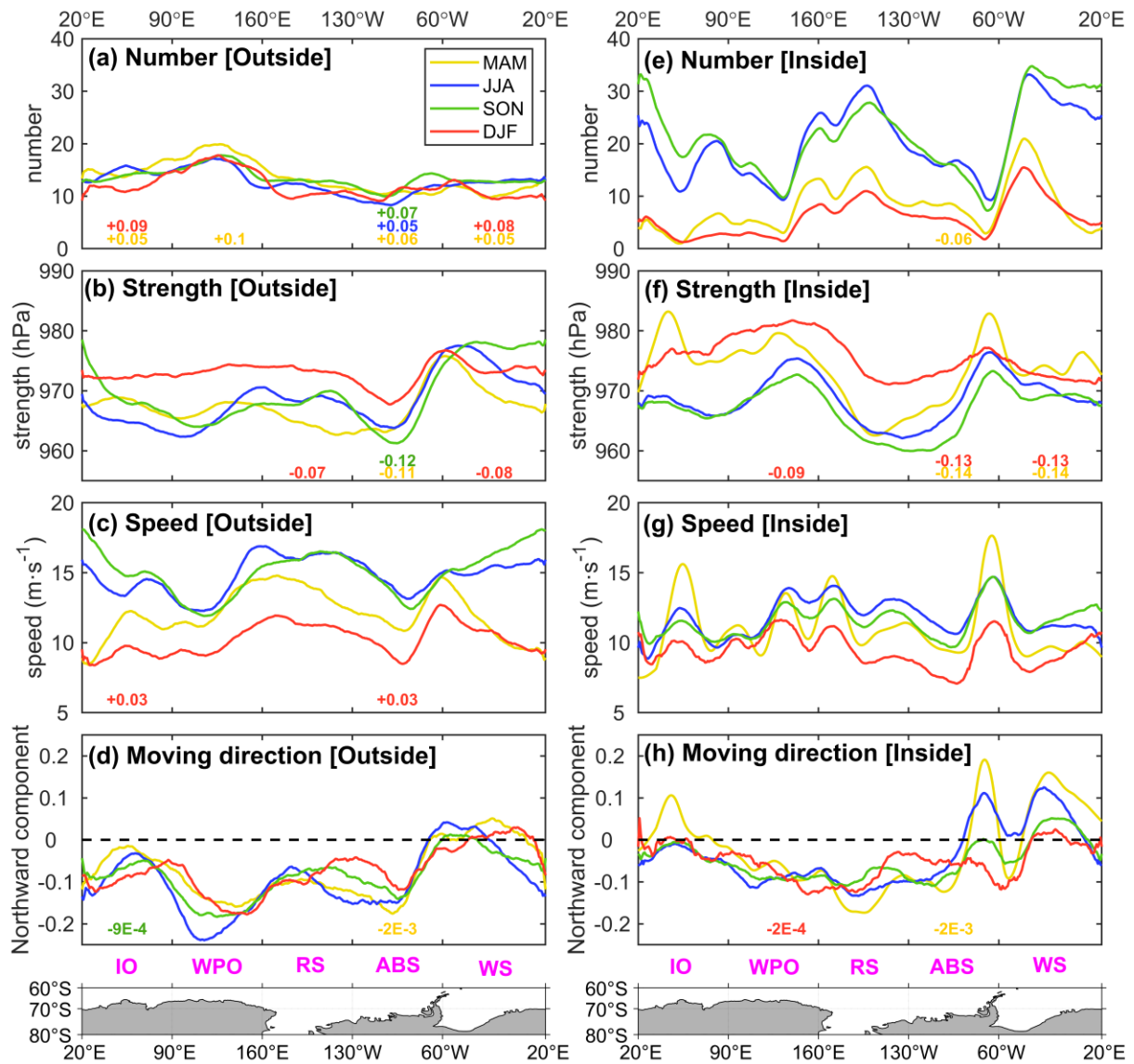
437 According to the methods described in methods section, we investigate the
438 characteristics of cyclones by dividing them into inside and outside groups to compare the
439 differences between cyclones inside and outside the sea ice edge. Surprisingly, the number of
440 outside cyclones remains fairly consistent across various seasons in most regions, except for a
441 10% larger number in the WPO sector in MAM and the ABS sector in SON (Figure 5a). The
442 seasonal latitudinal shift of the sea ice edge appears to primarily impact the number of inside
443 cyclones (Figure 5e). Larger seasonal differences in the number of inside cyclones are observed
444 not only in regions with extensive sea ice (RS and WS) but also in areas with narrower sea ice
445 extent (IO and WPO).

446 Seasonal and regional differences also exist in the strength (MSLP minima) of cyclones
447 (Figure 5b). A similar double peak can be seen in the WPO and ABS sectors in JJA and SON.
448 Conversely, cyclones exhibit stronger intensity in JJA than in SON in the WS-IO sector. Summer
449 (DJF) cyclones are notably less intense than their winter (JJA) counterparts in general. Notably, a
450 single peak in cyclone intensity is observed in the ABS region for outside cyclones in summer,
451 indicating that the cyclones here maintain stronger strength throughout the year. Furthermore,
452 the significant positive trend in the number and strength of cyclones in the ABS region, along
453 with their increased southward movement speed, may contribute to the notable decline in sea
454 ice in this region compared to others (Figure 4a).

455 In addition to the sea ice response to the number and strength of cyclones, sea ice may
456 also respond to varying cyclone translational speeds and trajectories. Slow-moving cyclones tend
457 to engage with sea ice over extended durations, resulting in more pronounced dynamic and
458 thermal effects on the ice. Outside cyclones generally move at speeds within a range of 7-18 m/s
459 (Figure 5c). The mean speed, partially dependent on the number of cyclones, also shows regional
460 and seasonal differences. The highest mean speeds manifest at 160°E during winter. The peaks
461 of the mean speed align with regions where sea ice extends northward, such as the Drake Passage
462 and Prydz Bay. Cyclones west of the Antarctic Peninsula typically have low speed and a larger
463 northward component in their motion. Most of them accelerate when they pass through the
464 Drake Passage and then turn southward (Figure 5d). The largest southward component appears
465 at 110°E, coinciding with peaks in number and strength. This implies that cyclones in this region
466 are more likely to intrude extensively into the sea ice, thereby imposing a more severe impact on
467 the ice. Another area that may have a severe impact is located in the ABS area, where cyclones
468 have large strength, slow speed, and large southward moving direction.

469 The seasonal variation of the sea ice edge has a great impact on the average feature of
470 inside cyclones, especially in the regions that have wide sea ice areas such as the RS, WS regions,
471 and Prydz Bay (Figure 5e). The large number of inside cyclones in these regions may weaken the
472 peak value of cyclone features, especially for the mean speed and southward component of
473 moving direction. Generally, their speed is also slower entering the sea ice edge due to the
474 influence of the continent and the circumpolar easterly winds (Figure 5g). Similar to outside
475 cyclones, there is an acceleration in the speed of inside cyclones west of the Antarctic Peninsula
476 accompanied by a pronounced northward motion component. Another northward passage
477 occurs around the primary meridian, beyond which most cyclones move south (Figure 5h). The

478 three peaks of the number of inside cyclones around 160°E, 170°W, and 45°W correspond to the
 479 three main cyclogenesis regions along the coast (Figure 5e), accompanied by frequent cold air
 480 outbreak events and strong katabatic winds (Parish & Cassano, 2003; Bromwich et al., 2011;
 481 Papritz et al., 2015). In other regions, the difference in numbers between JJA and DJF is mostly
 482 attributed to the expansion of the sea ice extent. Except for the larger numbers than outside
 483 cyclones, the intensity of inside cyclones also has two peaks around 90°E and 130°W and they
 484 last for two and three seasons respectively (Figure 5f). Cyclones within the narrow sea ice band
 485 in the IO-WPO sector do not have enough time and space to reach higher intensities in MAM.



486

487 **Figure 5.** Meridional-mean values of (a & e) cyclone count, (b & f) strength, (c & g) speed, and (d
 488 & h) moving direction (northward component) for ice-linked cyclones outside the sea ice edge
 489 (a-d) and inside the sea ice edge (e-h) during MAM (yellow line), JJA (blue line), SON (green line),
 490 and DJF (red line). Only smoothed results using a 30-point moving average are shown. Significant

491 trends (passing the 95% t-test level) are shown below the lines, with colors corresponding to the
492 respective seasons. Unit: per year.

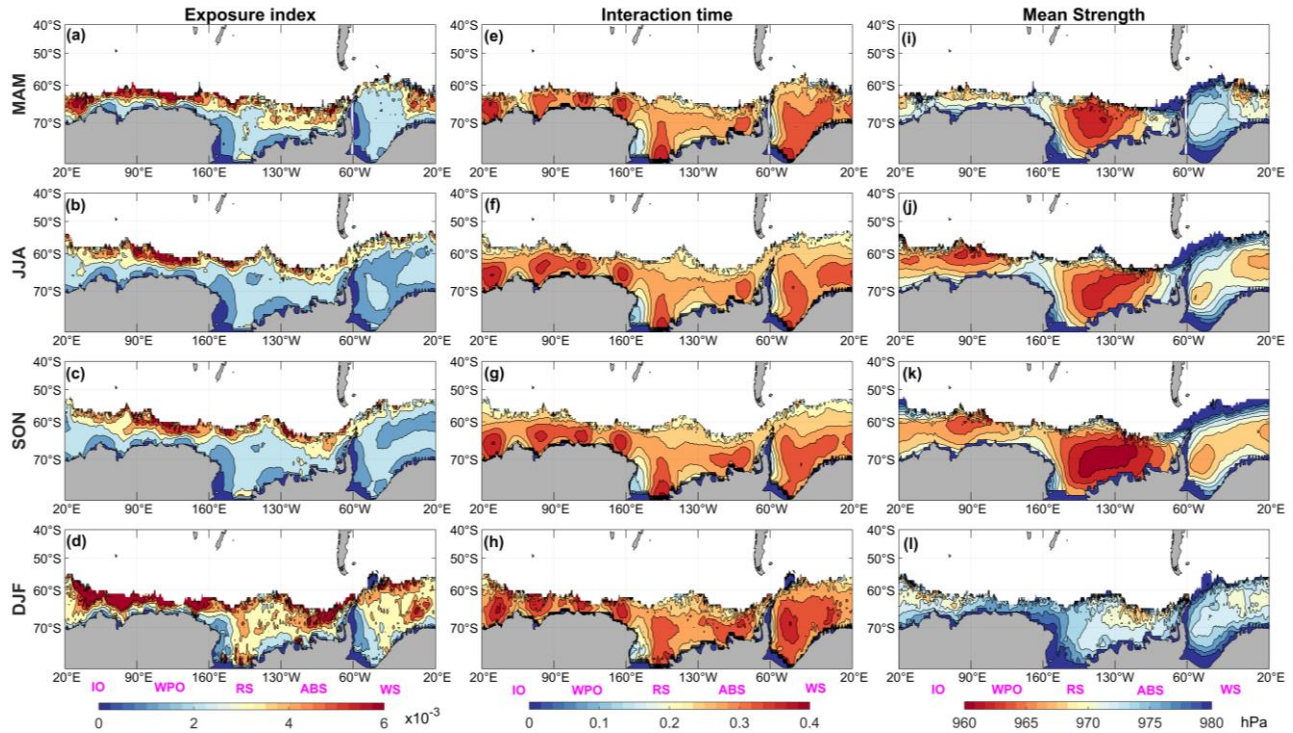
493

494 3.4 Index of sea ice exposure to cyclones

495 To comprehensively analyze the seasonal and regional relationship between cyclones and
496 sea ice, an exposure index has been developed to assess the impact of cyclones on sea ice (Data
497 and Method 2.3). The index accounts for the number and strength of passing cyclones, the
498 interaction time between sea ice and cyclones, and the local SIC. Typically, sea ice in areas with
499 low SIC and frequent cyclone activity, such as the marginal ice zone (MIZ: $0.15 < SIC < 0.75$), is
500 more susceptible to severe impact by cyclones. Therefore, a high-exposure belt is expected along
501 the sea ice edge in all four seasons, although seasonal and regional differences exist.

502 The highest exposure value is observed in the WPO sector, driven by the local feature of
503 a larger number of slow-moving cyclones and the largest southward component in their
504 movement direction (Figure 5a-d). The interaction time increases when there are a large number
505 of slow-moving cyclones (Figure 6e-h). Cyclones with greater strength are likely to be more
506 destructive to sea ice, particularly in the MIZ. When cyclones move across the sea ice edge and
507 enter the interior of the sea ice cover where $SIC > 0.9$, the exposure index decreases despite
508 longer interaction times and higher mean cyclone strength. This can be seen in the RS and WS
509 basins typically (Figure 6j-k). Slow-moving cyclones near the coast also increase the interaction
510 time. The exposure index in the RS and WS regions shows similar seasonal variations. Due to the
511 rapid retreat of sea ice in these two regions during DJF, more low-density ice areas emerge,
512 leading to a wider high-exposure area instead of a narrow belt seen in other seasons (Figure 6d).

513 The condition of the sea ice strongly influences the index. The Antarctic sea ice has a rapid
514 growth in MAM and a decline in DJF. In these two seasons, the exposure value is higher than that
515 in JJASON because more grid points with low SIC in MAM may be easily affected by the cyclones.
516 In general, SIC dominates the seasonal variation of the exposure index, while cyclones dominate
517 the regional differences in the exposure index. However, this is not an absolute conclusion. For
518 example, the small number of summer cyclones results in a lower exposure index in the MIZ
519 during DJF compared to other seasons, while the thick, old ice in the frontal ice zone of the RS
520 protects the sea ice from further cyclone impacts during JJA. Although cyclones with different
521 characteristics in different seasons cause significant differences in mean strength over sea ice
522 and interaction time, the response in the range and depth of high exposure in the MIZ is limited
523 after considering sea ice concentration. This variation in the exposure index may help explain
524 why the relationship is regional and seasonal, as well as identify the most noteworthy season for
525 each subregion.



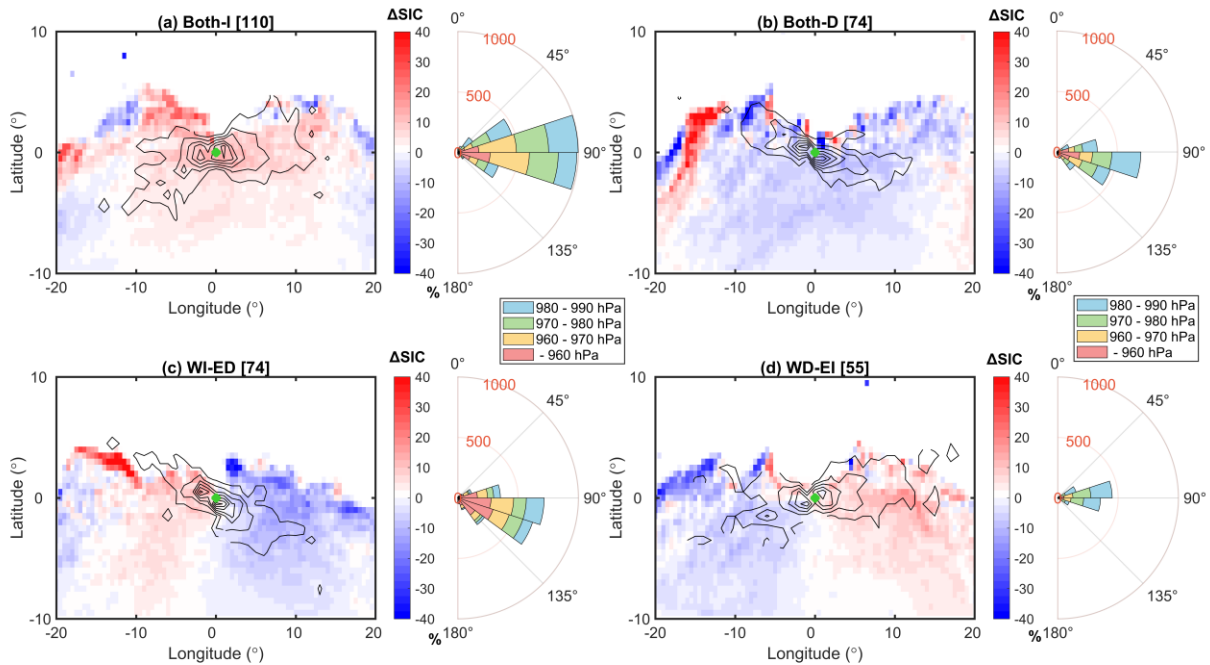
526

527 **Figure 6.** Panels (a–d) show the seasonal distributions of the normalized exposure index. Panels
 528 (e–h) present the mean normalized interaction time, calculated by dividing by 48 hours for ± 1 -
 529 day periods. Panels (i–l) display the mean strength of these cyclones. Each row corresponds to a
 530 different season, with season markers indicated on the far left.

531

532 3.5 SIC responses to cyclones

533 Following the analysis of cyclone characteristics and sea ice exposure above, regional and
 534 seasonal differences in the exposure of sea ice to cyclones have been identified. However, it
 535 remains uncertain whether the passage of a cyclone will lead to an increase or decrease in local
 536 SIC. To address this, it is necessary to examine the cumulative impact of each cyclone on the local
 537 sea ice using a SIC anomaly field around the cyclone center over a ± 1 day period. Given the limited
 538 movement of the cyclone, sea ice anomalies within ± 1 day can mainly be attributed to the cyclone
 539 itself. September ice-linked cyclones are selected for this composite analysis to mitigate the
 540 influence of seasonal sea ice growth/retreat and missing values over land on the results. These
 541 cyclones are categorized based on positive and negative sea ice anomalies on their eastern and
 542 western sides (Data and Method 2.4).



543

544 **Figure 7.** Composite results (shaded) of isolated cyclones in September, categorized as (a) Both-
 545 I, (b) Both-D, (c) WI-ED, and (d) WD-EI sea ice anomalies within ± 1 day. Track density is outlined
 546 in black contours, and cyclone centers are marked with green dots. The adjacent wind rose chart
 547 illustrates cyclone intensity (MSLP) and movement direction. The number of cyclones included in
 548 the composite analysis is indicated in square brackets in the title.

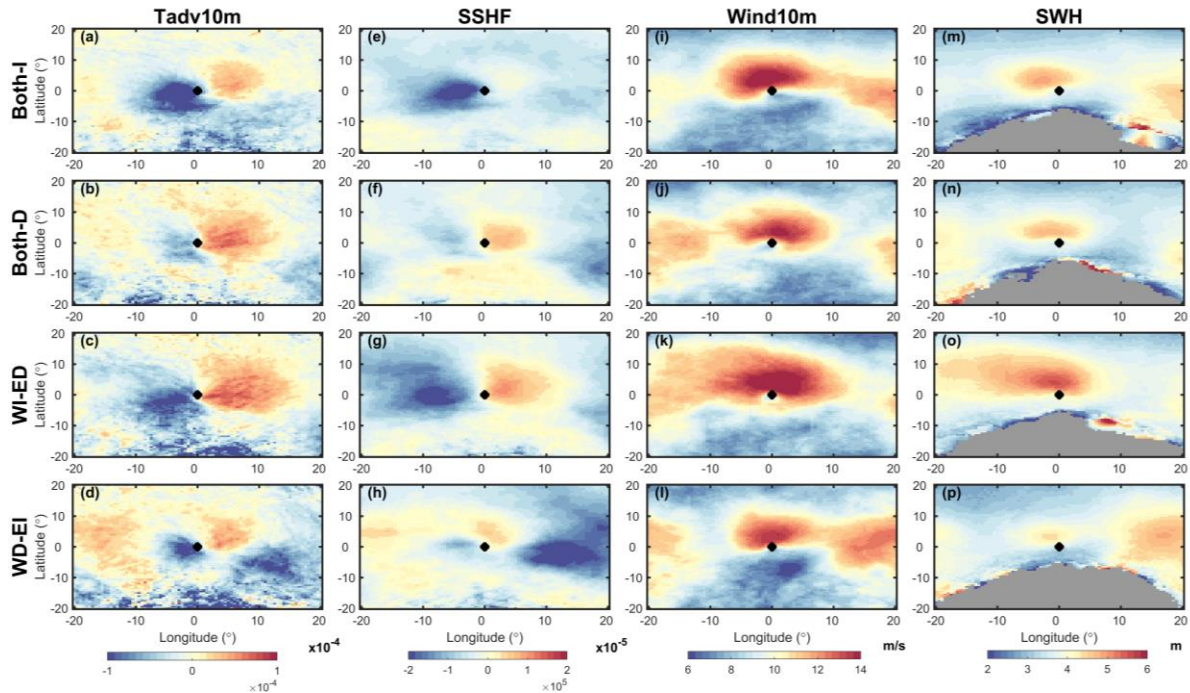
549

550 The composite focuses on isolated cyclones to avoid the influence of additional cyclones
 551 upstream or downstream on the composite results. Figure 7 shows the SIC composite results for
 552 four types of cyclones and their track features. On average, an isolated cyclone causes an
 553 anomaly of up to $\pm 40\%$ in SIC within two days, with significantly large anomalous values at the
 554 sea ice edge. In general, cyclones have a greater impact on the sea ice edge than on the interior,
 555 manifested by southward movement and extrusion of sea ice on the east side and northward
 556 movement with internal ice growth on the west side of the cyclone center. This results in a
 557 positive SIC anomaly on the west side and a negative SIC anomaly on the east side (WI-ED), with
 558 thermodynamic effects from the cyclonic circulation further reinforcing this pattern. The cyclone
 559 path influences the shape of the sea ice edge and anomaly distribution, with different paths
 560 observed in various cases (e.g., NW-SE path for Both-D and WI-ED cases, W-E path for Both-I and
 561 WD-EI cases).

562 The wind rose chart indicates that WI-ED cyclones are significantly stronger than Both-D
 563 cyclones during their interaction with sea ice, with nearly half of the time steps showing
 564 intensities below 970 hPa and one-third below 960 hPa. This strength difference explains the
 565 positive anomaly on the west side of WI-ED cyclones but not Both-D cyclones, even though both
 566 have similar NW-SE paths moving towards the interior of the sea ice (Figure 7b and 7c). A stronger
 567 WI-ED cyclone can drive more intense cold advection towards the equator on the west

568 (Figure 8c), leading to rapid sea ice growth. In contrast, the weaker Both-D cyclone lacks favorable
569 conditions for sea ice growth on its western side. There is either no or weak cold advection and
570 less surface sensible heat flux (SSHF) on the western side of the Both-D cyclone (Figure 8b and
571 8f). In terms of maximum wind speed and significant wave height, the distribution pattern is
572 similar for both cyclones, differing primarily in intensity (Figure 8i-j and 8n-o). Thus, it is
573 reasonable to infer that along an NW-SE path, a strong cyclone most likely induces a WI-ED sea
574 ice response, while a weak cyclone typically results in a Both-D response. The key factor
575 distinguishing them is the strength of cold advection and negative SSHF on the western side. Both
576 have large warm advection and positive SSHF on the eastern side, which distinguishes them from
577 the other two types of cyclones.

578 Comparing the Both-I and WD-EI cases, Both-I generally follows a W-E path (Figure 7a).
579 Along this path, the negative anomaly on the eastern side is partially offset by the positive
580 anomaly from offshore winds on the western side as the cyclone moves eastward, resulting in an
581 east-west increasing anomaly pattern over two days. As the cyclone moves eastward, the original
582 negative anomaly on the eastern side is offset. In terms of sensible heat flux, only the western
583 side exhibits a larger negative sensible heat flux, while the eastern side is close to 0 (Figure 8e).
584 These results are opposite to those observed in Both-D cyclones (Figure 8f). The WD-EI cases also
585 follow a W-E path but have more northward components (Figure 7d). Most WD-EI cases have
586 their genesis at the sea ice edge and move eastward afterward, resulting in significantly more
587 trajectory points on the eastern side than on the western side. Hence, the negative anomaly on
588 the western side may not be attributed solely to the cyclone itself. In Figure 8d, the range of cold
589 and warm advection for this cyclone type is much smaller than that for the other three types.
590 These cyclones, which develop by baroclinicity from air-ocean temperature differences at the ice
591 edge, are typically small- to mesoscale, with weaker intensity (Figure 7d) and cause the smallest
592 wind speeds and lowest wave heights among the three types (Figure 8l and 8p). This also raises
593 the question of whether such an abnormal WD-EI response is caused by the cyclone itself or the
594 background circulation, as evidenced by the stronger warm advection on the left and cold
595 advection on the right outside the cyclone's circulation, compared to the cyclone itself (Figure
596 8d).



597

598 **Figure 8.** Composite results (shaded) of environmental factors for different types of isolated
 599 cyclones in September. Panels (a–d) depict temperature advection at 10m, while panels (e–h)
 600 illustrate surface sensible heat flux. Panels (i–l) present wind speed at 10m, and panels (m–p)
 601 display significant wave height. Cyclone centers are marked with black dots.

602

603 4 Discussion

604 By categorizing cyclones based on SIC anomalies in this study, we provide a reasonable
 605 explanation for the weak correlation between Antarctic sea ice and cyclones on interannual and
 606 decadal **scales**. The relationship between cyclones and sea ice varies **annually** due to the differing
 607 proportions of the four types of SIC anomalies among cyclones. It is not straightforward to predict
 608 whether sea ice will **increase or decrease abnormally in years with unusually high or low cyclone**
 609 **activity**. The annual cycle of cyclone impacts on SIC is influenced by variations in cyclone intensity
 610 and the sea ice conditions they traverse (Aue et al., 2023a). A high number of cyclones does not
 611 necessarily indicate extreme sea ice extent. **However, case studies on the relationship between**
 612 **cyclones and extreme sea ice reduction events (e.g., Turner et al., 2017; 2022 in Antarctica;**
 613 **Simmonds and Rudeva, 2012; Zhang et al., 2013 in the Arctic) provide confidence in continuing**
 614 **to explore this relationship. At the very least, they allow us to summarize differences in cyclone**
 615 **characteristics and transport factor fields during the early stages of extreme sea ice years. This is**
 616 **particularly important in the context of global warming and the recurring record lows in Antarctic**
 617 **sea ice. Future research can begin by examining seasonal changes in sea ice. Based on previous**
 618 **findings, the circumpolar trough can influence sea ice growth (Eayrs et al., 2019), while cyclone**
 619 **location and local wind fields can drive extreme changes in local sea ice (Wang et al., 2014). In**
 620 **our other studies, we have found a relationship between the monthly advance speed of the sea**
 621 **ice edge and the number of the four types of cyclones. However, it remains necessary to quantify**

622 the net contribution of cyclones to sea ice growth and melting, beyond their role in the spatial
623 redistribution of sea ice.

624 Further investigation of the relationship between cyclones and extreme sea ice requires
625 careful screening of cyclones based on their characteristics, including their paths and intensities
626 as well their wind speed and direction. The current research still has some limitations, such as
627 the potential impact of ERA5 data bias, which can benefit from the comparative validation with
628 multiple data sets; The T42 spatial filtering used in cyclone tracking retains only synoptic scale
629 signals, resulting in the lack of small- and mesoscale cyclones in the dataset. These small-size
630 cyclones are mostly linked to cold air outbreaks and are also closely related to sea ice (Irving et
631 al., 2010); Only eastward-moving cyclones were selected in our study because they accounted
632 for 75% of all track points and had a significant increasing trend. In fact, the influence of different
633 directions of the cyclone on the anomalous sea ice concentration is **significant**, because its
634 asymmetrical wind field structure is accompanied by asymmetrical swells. In addition, the speed
635 of the cyclone may cause different sea ice anomalies. The fast eastward moving cyclone may have
636 little effect on sea ice, the positive sea ice anomaly caused by the offshore wind to the west will
637 offset the negative sea ice anomaly caused by the onshore wind to the east at the previous
638 moment, and the final accumulation will be a small impact. **Local sea ice changes can also result
639 from the cumulative effects of multiple cyclones, particularly during winter when cyclone activity
640 intensifies. Dynamic mechanisms dominate the SIC response during rapid succession of cyclones,
641 while longer gaps between cyclones before and after allow thermodynamic effects to lead in
642 refreezing (Aue et al., 2023b). The multiple impact of cyclone clusters are also need to further
643 investigate.** Therefore, we are interested in whether slow and strong cyclones and cyclone
644 clusters cause long-term changes in sea ice, since the number of such cyclones may have a
645 stronger relationship with the extreme sea ice extent events. It is quite challenging to identify
646 which **features** of cyclones lead to long-term changes in sea ice, resulting in extreme SIE events
647 in the following month or season, and finding reasonable physical mechanisms for this
648 correlation should be a focus of future work.

649

650 **5 Conclusions**

651 The sea ice around Antarctica undergoes a natural cycle of expansion and retreat, with
652 larger areas covered by sea ice during winter (JJA) and spring (SON), and smaller areas during
653 summer (DJF) and autumn (MAM). Regional variations exist in the positioning of the sea ice edge,
654 particularly in the Lazarev Sea and the Ross Sea, where significant north-south variations are
655 observed. Meanwhile, the **tracks** of Southern Ocean cyclones follow a circular pattern, with the
656 highest frequency observed around 60°S. The storm track shifts closer to the Antarctic continent
657 during the sea ice retreat period (ONDJF) and extends northward during the sea ice advance
658 period (MAMJJAS). However, the south-north shift of the storm track does not coincide with the
659 expansion and retreat of the sea ice edge, resulting in disparities in the number of track points
660 inside and outside the sea ice edge. Here, we show that both inside and outside cyclone track
661 points exhibit an increasing trend on a decadal timescale, although the increasing trend of sea
662 ice extent reverses after 2015. The correlation coefficient analysis further reveals no significant

663 relationship between the number of outside cyclones and the latitude of sea ice edge on a long-
664 term timescale. The shifting sea ice edge mainly affects the number of track points within the ice
665 edge, while the number of track points outside remains similar across most seasons. The strength
666 of cyclones also varies between regions and seasons, with wider sea ice areas allowing for further
667 development and longer lifetimes of cyclones inside the ice edge. The speed and direction of
668 cyclone movement should also be considered in the study of the relationship between cyclones
669 and sea ice.

670 Therefore, an exposure index was designed based on the features of cyclones, local sea
671 ice conditions, and the interaction time between them. A high-exposure belt exists along the sea
672 ice edge throughout the year. Regions with low SIC and frequent cyclones are more susceptible
673 to cyclone impacts. Regional and seasonal variations in the exposure index can be explained by
674 the features of cyclones. For example, the highest exposure occurs in the WPO sector due to local
675 cyclones with larger numbers, slower speeds, and southward movement. Generally, cyclones
676 with slower speeds have a greater impact on sea ice due to longer interaction times. The
677 exposure index map helps explain the regional and seasonal relationship between cyclones and
678 sea ice, highlighting noteworthy seasons for each subregion.

679 On this basis, we further focus on the response of SIC to cyclones at the sea ice edge. On
680 average, isolated cyclones can induce $\pm 40\%$ SIC anomalies within two days, particularly at the sea
681 ice edge. Along the same NW-SE path, stronger cyclones drive intense cold advection, causing a
682 WI-ED response, while weaker cyclones result in a Both-D response due to favorable conditions
683 for west-side sea ice growth. The W-E path of cyclones produces a Both-I response, with the
684 negative anomaly on the eastern side of the cyclone offset by the positive anomaly after the
685 cyclone passes through. In general, SIC anomaly distribution depends on the cyclone path,
686 intensity, and environmental factors such as temperature advection and surface sensible heat
687 flux. This provides a new perspective on short-term changes in sea ice driven by cyclones.

688 Overall, the variations in Antarctic sea ice and Southern Ocean cyclones are complex and
689 interconnected. The impact of cyclones on sea ice throughout their entire life cycle is **dynamic**,
690 depending on the characteristics and conditions of the sea ice below. Understanding the
691 dynamics and interactions between sea ice and cyclones, including the impact of cyclones on
692 ocean and sea ice properties, is crucial for accurately assessing their effects on sea ice extent and
693 variability. The trends in the number of cyclones and the latitude of the sea ice edge show
694 significant seasonal and regional variation, as does the proportion of cyclones outside and inside
695 the sea ice edge. The findings presented here provide valuable insights into these relationships,
696 which can contribute to understanding recent trends and variability in Antarctic sea ice, its
697 seasonal and regional characteristics, and the future effects of global warming and the poleward
698 shift of storm tracks on Antarctic sea ice.

699

700 **Acknowledgments**

701 This study was supported by the National Natural Science Foundation of China (No.
702 41941009) and the Southern Marine Science and Engineering Guangdong Laboratory (Zhuhai)
703 (Nos. SML2023SP217, SML2023SP219, SML2022SP401). We thank Kyle Clem at Victoria
704 University of Wellington for useful comments on the paper.
705

706 Open Research

707 Hourly ERA5 data are available at Hersbach et al. (2023a, 2023b) and they can be
708 downloaded from Climate Data Store of Copernicus Center (Two datasets: ERA5 hourly data on
709 single levels from 1940 to present and ERA5 hourly data on pressure levels from 1940 to present).
710 Southern Ocean cyclone dataset is available at Zhong et al. (2022). The code for the cyclone
711 detection and tracking algorithm can be found at <https://gitlab.act.reading.ac.uk/track/track>.
712

713 References

- 714 Aue, L., Vihma, T., Uotila, P., & Rinke, A. (2022). New insights into cyclone impacts on sea ice in
715 the Atlantic sector of the Arctic Ocean in winter. *Geophys. Res. Lett.*, *49*, e2022GL100051.
716 <https://doi.org/10.1029/2022GL100051>
- 717 Aue, L., & Rinke, A. (2023a). Cyclone impacts on sea ice concentration in the Atlantic Arctic Ocean:
718 Annual cycle and recent changes. *Geophys. Res. Lett.*, *50*, e2023GL104657.
719 <https://doi.org/10.1029/2023GL104657>
- 720 Aue, L., Röntgen, L., Dorn, W., Uotila, P., Vihma, T., Spreen, G., & Rinke, A. (2023b). Impact of
721 three intense winter cyclones on the sea ice cover in the Barents Sea: A case study with a
722 coupled regional climate model. *Front. Earth Sci.*, *11*, 1112467.
723 <https://doi.org/10.3389/feart.2023.1112467>
- 724 Bromwich, D., Steinhoff, D., Simmonds, I., Keay, K., & Fogt, R. (2011). Climatological aspects of
725 cyclogenesis near Adélie Land, Antarctica. *Tellus*, *63A*, 921–938.
726 <https://doi.org/10.1111/j.1600-0870.2011.00537.x>
- 727 Carleton, A. (1983). Variations in Antarctic sea ice conditions and relationships with Southern
728 Hemisphere cyclonic activity, winters 1973-77. *Arch. Meteorol. Geophys. Bioclimatol. Ser. B*
729 *Theor. Appl. Climatol.*, *32*, 1–22. <https://doi.org/10.1007/BF02269387>
- 730 Carleton, A., & Carpenter, D. (1989). Intermediate-scale sea ice—atmosphere interactions over
731 high southern latitudes in winter. *GeoJournal*, *18*, 87–101.
732 <https://doi.org/10.1007/BF00722392>
- 733 Clancy, R., Bitz, C. M., Blanchard-Wrigglesworth, E., McGraw, M. C. & Cavallo, S. M. (2022). A
734 cyclone-centered perspective on the drivers of asymmetric patterns in the atmosphere and
735 sea ice during Arctic cyclones. *J. Climate*, *35*, 73–89. <https://doi.org/10.1175/JCLI-D-21-0093.1>
- 736 Clem, K., Massom, R., Stammerjohn, S., & Reid, P. (2022). Antarctic sea ice #2: Biological
737 importance. *Antarctic Environments Portal*. <https://doi.org/10.48361/8TKY-2793>
- 738 Dare, R., & Atkinson, B. (1999). Numerical modeling of atmospheric response to polynyas in the
739 Southern Ocean sea ice zone. *J. Geophys. Res.*, *104*, 16691–16708.
740 <https://doi.org/10.1029/1999JD900137>

- 741 Eastwood, S., Lavergne, T., & Tonboe, R. (2014). Algorithm theoretical basis document for the
 742 OSI SAF global reprocessed sea ice concentration product, version 1.1. EUMETSAT Satellite
 743 Application Facilities, Darmstadt, Germany.
- 744 Eayrs, C., Holland, D., Francis, D., Wagner, T., Kumar, R., & Li, X. (2019). Understanding the
 745 seasonal cycle of Antarctic sea ice extent in the context of longer-term variability. *Reviews of*
 746 *Geophysics*, *57*, 1037–1064. <https://doi.org/10.1029/2018RG000631>
- 747 Eayrs, C., Li, X., Raphael, M., & Holland, D. (2021). Rapid decline in Antarctic sea ice in recent
 748 years hints at future change. *Nat. Geosci.*, *14*, 460–464. [https://doi.org/10.1038/s41561-021-](https://doi.org/10.1038/s41561-021-00768-3)
 749 [00768-3](https://doi.org/10.1038/s41561-021-00768-3)
- 750 Finocchio, P., Doyle, J., Stern, D., & Fearon, M. (2020). Short-term impacts of Arctic summer
 751 cyclones on sea ice extent in the marginal ice zone. *Geophys. Res. Lett.*, *47*, e2020GL088338.
 752 <https://doi.org/10.1029/2020GL088338>
- 753 Finocchio, P., Doyle, J., & Stern, D. (2022). Accelerated sea ice loss from late summer cyclones in
 754 the new Arctic. *J. Climate*, *35*, 7751–7769. <https://doi.org/10.1175/JCLI-D-22-0315.1>
- 755 Francis, D., Eayrs, C., Cuesta, J., & Holland, D. (2019). Polar cyclones at the origin of the
 756 reoccurrence of the Maud Rise Polynya in austral winter 2017. *J. Geophys. Res.: Atmospheres*,
 757 *124*, 5251–5267. <https://doi.org/10.1029/2019JD030618>
- 758 Godfred-Spenning, C., & Simmonds, I. (1996). An analysis of Antarctic sea-ice and extratropical
 759 cyclone associations. *Int. J. Climatol.*, *16*, 1315–1332. [https://doi.org/10.1002/\(SICI\)1097-](https://doi.org/10.1002/(SICI)1097-0088(199612)16:12<1315::AID-JOC92>3.0.CO;2-M)
 760 [0088\(199612\)16:12<1315::AID-JOC92>3.0.CO;2-M](https://doi.org/10.1002/(SICI)1097-0088(199612)16:12<1315::AID-JOC92>3.0.CO;2-M)
- 761 Hepworth, E., Messori, G., & Vichi, M. (2024). Synoptic-scale extreme variability of winter
 762 Antarctic sea-ice concentration and its link to Southern Ocean extratropical cyclones. *J.*
 763 *Geophys. Res.: Oceans*, *129*, e2023JC019825. <https://doi.org/10.1029/2023JC019825>
- 764 Hersbach, H., et al. (2020). The ERA5 global reanalysis. *Quart. J. Roy. Meteor. Soc.*, *146*, 1999–
 765 2049. <https://doi.org/10.1002/qj.3803>
- 766 Hersbach, H., et al. (2023a). ERA5 hourly data on pressure levels from 1940 to present [Dataset].
 767 Copernicus Climate Change Service (C3S) Climate Data Store (CDS).
 768 <https://doi.org/10.24381/cds.bd0915c6>
- 769 Hersbach, H., et al. (2023b). ERA5 hourly data on single levels from 1940 to present [Dataset].
 770 Copernicus Climate Change Service (C3S) Climate Data Store (CDS).
 771 <https://doi.org/10.24381/cds.adbb2d47>
- 772 Hirahara, S., Balmaseda, M., Boisseson, E., et al. (2016). Sea surface temperature and sea ice
 773 concentration for ERA5. Eur. Centre Medium Range Weather Forecasts, Berkshire, UK, ERA
 774 Rep. Ser, 26.
- 775 Hobbs, W., Massom, R., Stammerjohn, S., Reid, P., Williams, G., & Meier, W. (2016). A review of
 776 recent changes in Southern Ocean sea ice, their drivers and forcings. *Global Planet. Change*,
 777 *143*, 228–250. <https://doi.org/10.1016/j.gloplacha.2016.06.008>
- 778 Hodges, K. (1994). A general method for tracking analysis and its application to meteorological
 779 data. *Mon. Wea. Rev.*, *122*, 2573–2586. [https://doi.org/10.1175/1520-](https://doi.org/10.1175/1520-0493(1994)122<2573>2.0.CO;2)
 780 [0493\(1994\)122<2573>2.0.CO;2](https://doi.org/10.1175/1520-0493(1994)122<2573>2.0.CO;2)
- 781 Hodges, K. (1995). Feature tracking on the unit sphere. *Mon. Wea. Rev.*, *123*, 3458–3465.
 782 [https://doi.org/10.1175/1520-0493\(1995\)123<3458>2.0.CO;2.](https://doi.org/10.1175/1520-0493(1995)123<3458>2.0.CO;2)

- 783 Hodges, K. (1999). Extension of spherical nonparametric estimators to nonisotropic kernels: An
784 oceanographic application. *Mon. Wea. Rev.*, *127*, 214–227. [https://doi.org/10.1175/1520-0493\(1999\)127<0214>2.0.CO;2](https://doi.org/10.1175/1520-0493(1999)127<0214>2.0.CO;2).
785
- 786 Hoskins, B. J. & Hodges, K. I. (2005). A New Perspective on Southern Hemisphere Storm Tracks.
787 *Journal of Climate*, *18*, 4108–4129. <https://doi.org/10.1175/JCLI3570.1>
788
- 789 Howarth, D. (1983). An analysis of the variability of cyclones around Antarctica and their
790 relationship to sea-ice extent. *Ann. Assoc. Am. Geogr.*, *73*, 519–537.
791 <https://doi.org/10.1111/j.1467-8306.1983.tb01856.x>
- 792 Irving, D., Simmonds, I., & Keay, K. (2010). Mesoscale cyclone activity over the ice-free Southern
793 Ocean: 1999–2008. *J. Climate*, *23*, 5404–5420. <https://doi.org/10.1175/2010JCLI3628.1>
794
- 795 Ionita, M., Scholz, P., Grosfeld, K., & Treffeisen, R. (2018). Moisture transport and Antarctic sea
796 ice: Austral spring 2016 event. *Earth System Dynamics*, *9*, 939–954.
797 <https://doi.org/10.5194/esd-9-939-2018>
- 798 Jena, B., Bajish, C., Turner, J., Ravichandran, M., Kshitija, S., Kumar, A., et al. (2022). Mechanisms
799 associated with the rapid decline in sea ice cover around a stranded ship in the Lazarev Sea,
800 Antarctica. *Sci. Total Environ.*, *821*, 153379. <https://doi.org/10.1016/j.scitotenv.2022.153379>
- 801 Jena, B., Bajish, C. C., Turner, J., Ravichandran, M., Kumar, A. N., & Kshitija, S. (2022). Record low
802 sea ice extent in the Weddell Sea, Antarctica in April/May 2019 driven by explosive polar
803 cyclones. *Climate and Atmospheric Science*, *5*, 19. <https://doi.org/10.1038/s41612-022-00243-9>
- 804 Jena, B., Kshitija, S., Bajish, C. C., Turner, J., Holmes, C., Wilkinson, J., Mohan, R., & Thamban, M.
805 (2024). Evolution of Antarctic sea ice ahead of the record low annual maximum extent in
806 September 2023. *Geophys. Res. Lett.*, *51*, e2023GL107561.
<https://doi.org/10.1029/2023GL107561>
- 807 Jones, J., Gille, S., Goose, H., et al. (2016). Assessing recent trends in high-latitude Southern
808 Hemisphere surface climate. *Nature Clim Change*, *6*, 917–926.
809 <https://doi.org/10.1038/nclimate3103>
- 810 Jenkins, M., & Dai, A. (2022). Arctic climate feedbacks in ERA5 reanalysis: Seasonal and spatial
811 variations and the impact of sea-ice loss. *Geophysical Research Letters*, *49*, e2022GL099263.
812 <https://doi.org/10.1029/2022GL099263>
- 813 Maksym, T. (2019). Arctic and Antarctic sea ice change: contrasts, commonalities, and causes.
814 *Annual Review of Marine Science*, *11*, 187–213. <https://doi.org/10.1146/annurev-marine-010816-060610>
815
- 816 Meehl, G. A., Arblaster, J. M., Chung, C. T. Y., Holland, M. M., DuVivier, A., Thompson, L., Yang,
817 D., & Bitz, C. M. (2019). Sustained ocean changes contributed to sudden Antarctic sea ice
818 retreat in late 2016. *Nature Communication*, *10*, 14. <https://doi.org/10.1038/s41467-018-07865-9>.
819

- 820 Menéndez, C., Serafini, V., & Le Treut, H. (1999). The effect of sea-ice on the transient
821 atmospheric eddies of the Southern Hemisphere. *Climate Dynamics*, *15*, 659–671.
822 <https://doi.org/10.1007/s003820050308>
- 823 Nghiem, S. V., Rigor, I. G., Clemente-Colón, P., Neumann, G., & Li, P. P. (2016). Geophysical
824 constraints on the Antarctic sea ice cover. *Remote Sensing of Environment*, *181*, 281–292.
825 <https://doi.org/10.1016/j.rse.2016.04.005>
- 826 Parish, T., & Cassano, J. (2003). The role of katabatic winds on the Antarctic surface wind regime.
827 *Mon. Wea. Rev.*, *131*, 317–333. [https://doi.org/10.1175/1520-0493\(2003\)131<0317>2.0.CO;2](https://doi.org/10.1175/1520-0493(2003)131<0317>2.0.CO;2)
- 828 Papritz, L., Pfahl, S., Sodemann, H., & Wernli, H. (2015). A climatology of cold air outbreaks and
829 their impact on air–sea heat fluxes in the high-latitude South Pacific. *J. Climate*, *28*, 342–364.
830 <https://doi.org/10.1175/JCLI-D-14-00482.1>
- 831 Parkinson, C., & Cavalieri, D. (2012). Antarctic sea ice variability and trends, 1979–2010.
832 *Cryosphere*, *6*, 871–880. <https://doi.org/10.5194/tc-6-871-2012>
- 833 Parkinson, C., & Comiso, J. (2013). On the 2012 record low Arctic sea ice cover: Combined impact
834 of preconditioning and an August storm. *Geophys. Res. Lett.*, *40*, 1356–1361.
835 <https://doi.org/10.1002/grl.50349>
- 836 Parkinson, C., & DiGirolamo, N. (2016). New visualizations highlight new information on the
837 contrasting Arctic and Antarctic sea-ice trends since the late 1970s. *Remote Sensing of*
838 *Environment*, *183*, 198–204. <https://doi.org/10.1016/j.rse.2016.05.020>
- 839 Parkinson, C. (2019). A 40-y record reveals gradual Antarctic sea ice increases followed by
840 decreases at rates far exceeding the rates seen in the Arctic. *Proceedings of the National*
841 *Academy of Sciences*, *116*, 14414–14423. <https://doi.org/10.1073/pnas.1906556116>
- 842 Parkinson, C., & DiGirolamo, N. (2021). Sea ice extents continue to set new records: Arctic,
843 Antarctic, and global results. *Remote Sensing of Environment*, *267*, 112753.
844 <https://doi.org/10.1016/j.rse.2021.112753>
- 845 Perlwitz, J. (2011). Tug of war on the jet stream. *Nature Clim Change*, *1*, 29–31.
846 <https://doi.org/10.1038/nclimate1065>
- 847 Petty, A., Stroeve, J., Holland, P., Boisvert, L., Bliss, A., Kimura, N., & Meier, W. (2018). The Arctic
848 sea ice cover of 2016: a year of record-low highs and higher-than-expected lows. *The*
849 *Cryosphere*, *12*, 433–452. <https://doi.org/10.5194/tc-12-433-2018>
- 850 Pezza, A., Durrant, T., Simmonds, I., & Smith, I. (2008). Southern Hemisphere synoptic behavior
851 in extreme phases of SAM, ENSO, sea ice extent, and Southern Australia rainfall. *J. Climate*,
852 *21*, 5566–5584. <https://doi.org/10.1175/2008JCLI2128.1>

- 853 Pirti, A., Yucel, M., & Hoşbaş, R. (2012). Displacement of the South Pole from 2006 to 2021: Role
854 of sea ice and Antarctic surface temperature. *Czech Polar Reports*, *12*, 203–221.
855 <https://doi.org/10.5817/CPR2022-2-15>
- 856 Ponce de León, S., & Bettencourt, J. H. (2021). Composite analysis of North Atlantic extra-tropical
857 cyclone waves from satellite altimetry observations. *Adv. Space Res.*, *68*, 762–772, <https://doi.org/10.1016/j.asr.2019.07.021>
858
- 859 Rudeva, I., & Gulev, S. K. (2011). Composite analysis of North Atlantic extratropical cyclones in
860 NCEP–NCAR reanalysis data. *Mon. Wea. Rev.*, *139*, 1419–1446, [https://doi.org/10.1175/](https://doi.org/10.1175/2010MWR3294.1)
861 [2010MWR3294.1](https://doi.org/10.1175/2010MWR3294.1)
- 862 Schemm, S. (2018). Regional trends in weather systems help explain Antarctic sea ice trends.
863 *Geophys. Res. Lett.*, *45*, 7165–7175. <https://doi.org/10.1029/2018GL079109>
- 864 Schroeter, S., O’Kane, T. J., & Sandery, P. A. (2023). Antarctic sea ice regime shift associated with
865 decreasing zonal symmetry in the Southern Annular Mode. *The Cryosphere*, *17*, 701–717.
866 <https://doi.org/10.5194/tc-17-701-2023>
- 867 Serreze, M., & Stroeve, J. (2015). Arctic sea ice trends, variability and implications for seasonal
868 ice forecasting. *Philosophical Transactions of the Royal Society A: Mathematical, Physical and*
869 *Engineering Sciences*, *373*, 20140159. <https://doi.org/10.1098/rsta.2014.0159>
- 870 Simmonds, I., & Wu, X. (1993). Cyclone behaviour response to changes in winter Southern
871 Hemisphere sea-ice concentration. *Q.J.R. Meteorol. Soc.*, *119*, 1121–1148.
872 <https://doi.org/10.1002/qj.49711951313>
- 873 Simmonds, I. (1996). Climatic role of Southern Hemisphere extratropical cyclones and their
874 relationship with sea ice. *Papers and Proceedings of the Royal Society of Tasmania*, *130*, 95–
875 100. <https://doi.org/10.26749/rstpp.130.2.95>
- 876 Simmonds, I. (2003). Regional and large-scale influences on Antarctic Peninsula climate. In
877 Antarctic Peninsula climate variability: historical and paleoenvironmental perspectives, *79*,
878 31–42. <https://doi.org/10.1029/AR079p0031>
- 879 Simmonds, I., & Rudeva, I. (2012). The great Arctic cyclone of August 2012. *Geophys. Res. Lett.*,
880 *39*, L23709. <https://doi.org/10.1029/2012GL054259>
- 881 Stammerjohn, S., & Maksym, T. (2017). Gaining (and losing) Antarctic sea ice: variability, trends
882 and mechanisms. In *Sea Ice*, ed. D. N. Thomas, pp. 261–89. Chichester, UK: Wiley & Sons.
- 883 Stoll, P. J. (2022). A global climatology of polar lows investigated for local differences and wind-
884 shear environments. *Weather and Climate Dynamics*, *3*, 483–504.
885 <https://doi.org/10.5194/wcd-3-483-2022>

- 886 Streten, N. (1983). Antarctic sea ice and related atmospheric circulation during FGGE. *Arch. Met.*
887 *Geoph. Biocl. A.*, 32, 231–246. <https://doi.org/10.1007/BF02291894>
- 888 Stuecker, M. F., Bitz, C. M., & Armour, K. C. (2017). Conditions leading to the unprecedented low
889 Antarctic sea ice extent during the 2016 austral spring season. *Geophys. Res. Lett.*, 44, 9008–
890 9019. <https://doi.org/10.1002/2017GL075017>
- 891 Titchner, H., & Rayner, N. (2014). The Met Office Hadley Centre sea ice and sea surface
892 temperature data set, version 2: 1. Sea ice concentrations. *Journal of Geophysical Research:*
893 *Atmospheres*, 119, 2864–2889. <https://doi.org/10.1002/2013JD020316>
- 894 Turner, J., Phillips, T., Marshall, G., Hosking, J., Pope, J., Bracegirdle, T., & Deb, P. (2017).
895 Unprecedented springtime retreat of Antarctic sea ice in 2016. *Geophys. Res. Lett.* 44, 6868–
896 6875. <https://doi.org/10.1002/2017GL073656>
- 897 Turner, J., Holmes, C., Caton Harrison, T., Phillips, T., Jena, B., Reeves-Francois, T., et al. (2022).
898 Record Low Antarctic Sea Ice Cover in February 2022. *Geophys. Res. Lett.*, 49.
899 <https://doi.org/10.1029/2022GL098904>
- 900 Uotila, P., Vihma, T., Pezza, A., Simmonds, I., Keay, K., & Lynch, A. (2011). Relationships between
901 Antarctic cyclones and surface conditions as derived from high-resolution numerical weather
902 prediction data. *J. Geophys. Res.*, 116, D07109. <https://doi.org/10.1029/2010JD015358>
- 903 Vichi, M., Eayrs, C., Alberello, A., Bekker, A., Bennetts, L., Holland, D., et al. (2019). Effects of an
904 explosive polar cyclone crossing the Antarctic marginal ice zone. *Geophys. Res. Lett.*, 46, 5948–
905 5958. <https://doi.org/10.1029/2019gl082457>
- 906 Vihma, T. (2014). Effects of Arctic Sea Ice Decline on Weather and Climate: A Review. *Surv*
907 *Geophys*, 35, 1175–1214. <https://doi.org/10.1007/s10712-014-9284-0>
- 908 Wang, Z., Turner, J., Sun, B., Li, B., & Liu, C. (2014). Cyclone-induced rapid creation of extreme
909 Antarctic sea ice conditions. *Sci. Rep.*, 4, 5317. <https://doi.org/10.1038/srep05317>
- 910 Wang, X., Zhang, Z., Wang, X., Vihma, T., Zhou, M., Yu, L., Uotila, P., & Sein, D. (2021). Impacts of
911 strong wind events on sea ice and water mass properties in Antarctic coastal polynyas. *Clim.*
912 *Dyn.*, 57, 3505–3528. <https://doi.org/10.1007/s00382-021-05878-7>
- 913 Wang, J., Luo, H., Yang, Q., Liu, J., Yu, L., Shi, Q., & Han, B. (2022). An Unprecedented Record Low
914 Antarctic Sea-ice Extent during Austral Summer 2022. *Advances in Atmospheric Sciences*, 39,
915 1591–1597. <https://doi.org/10.1007/s00376-022-2087-1>
- 916 Wang, X., Zhang, Z., Dinniman, M., Uotila, P., Li, X., & Zhou, M. (2023). The response of sea ice
917 and high-salinity shelf water in the Ross Ice Shelf Polynya to cyclonic atmosphere circulations.
918 *The Cryosphere*, 17, 1107–1126. <https://doi.org/10.5194/tc-17-1107-2023>
- 919 Ward, J. L., Payne, A. E., & Pettersen, C. (2023). Present-day regional Antarctic Sea Ice response
920 to extratropical cyclones. *Journal of Geophysical Research: Atmospheres*, 128,
921 e2023JD038914. <https://doi.org/10.1029/2023JD038914>
- 922 Watkins, A. B., & Simmonds, I. (1995). Sensitivity of numerical prognoses to Antarctic sea ice
923 distribution. *J. Geophys. Res.*, 100, 22681–22696. <https://doi.org/10.1029/95JC02581>
- 924 Watkins, A., & Simmonds, I. (1998). Relationships between Antarctic sea-ice concentration, wind
925 stress and temperature temporal variability, and their changes with distance from the coast.
926 *Annals of Glaciology*, 27, 409–412. <https://doi.org/10.3189/1998AoG27-1-409-412>
- 927 Yuan, X., Martinson, D., & Liu, W. (1999). Effect of air-sea-ice interaction on winter 1996 Southern
928 Ocean subpolar storm distribution. *J. Geophys. Res.*, 104, 1991–2007.
929 <https://doi.org/10.1029/98JD02719>

- 930 Zhang, J., Lindsay, R., Schweiger, A., & Steele, M. (2013). The impact of an intense summer
931 cyclone on 2012 Arctic sea ice retreat. *Geophys. Res. Lett.*, *40*, 720–726.
932 <https://doi.org/10.1002/grl.50190>
- 933 Zhang, L., Ren, X., Wang, C. Y., et al. (2024). An observational study on the interactions between
934 storm tracks and sea ice in the Southern Hemisphere. *Clim. Dyn.*, *62*, 17–36.
935 <https://doi.org/10.1007/s00382-023-06894-5>
- 936 Zhong, R., Yang, Q., Hodges, K., Wu, R., & Chen, D. (2022). Impact of Data Resolution on Tracking
937 Southern Ocean Cyclones. *Mon. Wea. Rev.*, *151*, 3–22. <https://doi.org/10.1175/MWR-D-22-0121.1>
- 938
939 Zwally, H., Comiso, J., Parkinson, C., Cavalieri, D., & Gloersen, P. (2002). Variability of Antarctic
940 sea ice 1979-1998. *J. Geophys. Res.*, *107*, 3041. <https://doi.org/10.1029/2000JC000733>
941